Advanced Engineering Science
http://publish.mersin.edu.tr/index.php/ades
e-ISSN 2791-8580

Determination of compaction parameters by image analysis technique

Atila Demiröz [*1], Mücahit Barstugan [2], Onur Saran [1], Hurşit Battal [1]

[1]*Konya Technical University, Department of Civil Engineering, Konya, Türkiye, ademiroz@ktun.edu.tr, osaran@ktun.edu.tr, hrsbattal@gmail.com*
[2]*Konya Technical University, Department of Electrical and Electronics Engineering, Konya, Türkiye, mbarstugan@ktun.edu.tr*

Cite this study: Demiröz, A., Barstugan, M., Saran, O. & Battal, H. (2023). Determination of compaction parameters by image analysis technique. Advanced Engineering Science, 3, 137-150

Keywords
Compaction
Image analysis
Void ratio

Research Article
Received:24.08.2023
Revised: 25.09.2023
Accepted: 11.10.2023
Published:19.10.2023

Abstract

In this study, the control of compaction parameters for a stabilized filling material that is used in Granular Subbase (GSB) construction was examined by image analysis. Whether the specimen coming from the field met the GSB conditions was checked, and its void ratio was examined by image analysis. For this process, the specimens that were prepared by mixing epoxy at different ratios were cut from a certain distance. Photographs were taken from the cut pieces using a SONY HSC-400 camera. For this purpose, specimens containing epoxy by 4%, 6%, 8%, and 10% were prepared. The ratios of the void found on the cut specimens were calculated. The void ratios that were calculated by using the e_{global} formula and those calculated by image processing methods were compared, and the void ratio was determined at an accuracy rate of 86.12% for the specimen that contained epoxy at a ratio of 8%.

1. Introduction

Depending on the use case, soil properties may not have the desired or expected qualities. In such a situation, to make the desired properties suitable for the use case, the geotechnical properties of the soil can be improved. The method of soil improvement varies based on the type and condition of the soil in the area. The purpose of all improvement (stabilization) techniques is to achieve a certain soil density, reduce the soil's permeability and subsidence, and increase its strength. As one of such improvement methods, compaction is used to increase the density and bearing capacity and lower its permeability [1].

In the compaction of soil in the field, vibratory, sheepsfoot, and rubber-tired rollers are used. In the laboratory, compaction is achieved by using the standard and modified Proctor experiments. In general, the compaction of clayey soils is dependent on the dry unit weight, water content, compaction energy, and the granulometry of the soil.

The most important point on the compaction curve is the peak point which is also called the optimum compaction point (OCP). This point determines two main parameters. These are the maximum dry density or dry unit weight (γ_{dmax}) and the corresponding optimum water content (w_{opt}).

To determine the engineering and index properties of the soil, data that are obtained as a result of various experiments in the laboratory are used. However, in this practice, the results that are obtained remain inadequate due to factors such as time, cost, equipment, and the difficulty of specimen collection. For this reason, in the literature, researchers have used correlation and regression analysis that can determine soil properties more easily and image processing methods that are constantly becoming more prevalent today. The approaches allow researchers to reach results on soil properties with fewer data points, at a low cost, and in the shortest time.

Until now, several scientific studies have been conducted on the image processing technique and compaction. Joslin [2] developed a highly popular method with the help of a water content-dry unit weight point determined

with the Standard Proctor experiment consisting of 26 different compaction curves. Latta and Leonard [3] reported that stabilization can be achieved by injecting epoxy into the soil at the optimum water content value. This is why they concluded that such an application can be made for the subbase, base, and surface layers of roads or airport runways. Nagaraj [4] developed a linear regression model that allows the approximation of the compaction curve of the soil based on its liquid limit value for liquid limits (WL) of 38-78%. Frost and Kuo [5] described an automated application of Oda's model that uses advanced image processing techniques. The proposed model eliminates the decision of the operator and manual operation and allows the confirmation of both the replicability and efficiency of the local void ratio distribution based on 2D plane cross-sections. Blotz et al. [6] determined the relationship between wopt and γdmax by using the experimental results of 22 clayey soil samples at different compaction energies for fine-grained soils. Using their data and other data in the literature for Standard Proctor compaction experiments on fine-grained soils, Sridharan and Nagaraj [7] obtained empirical formulae relating wopt and γdmax to WL and WP. Onal and Ozden [8] investigated granulometric parameters according to sieve analysis results using the digital image analysis method. Soycan [9] used compaction parameters obtained from Standard and Modified Proctor experiments on fine-grained soils and the index properties of soils to determine the maximum dry unit weight and optimum water content of the soils through artificial neural network analysis. Deb et al. [10] investigated changes in the compaction parameters of poorly graded sandy soil with the addition of fine-grained soil. Sezer et al. [11] examined changes in the local void ratios of granular soils compacted at different compaction energies by conducting experiments. The voids of the compacted soils were filled with epoxy, and void ratios were determined through image processing analysis. Bessa et al. [12] conducted various studies to characterize the microstructures of aggregates and hot mix asphalts by digital image processing. Cankaya et al. [13] produced a compressive strength prediction model with the image processing technique for determining concrete strength. They examined the parameters affecting concrete strength and their effect percentages. They observed that the image analysis results and the actual concrete strength values were very close. Oren [14] conducted analysis to predict the compaction parameters of fine-grained soils based on Atterberg limits and clay percentages. Santos et al. [15] established prediction models by analyzing the relationship between water content and the spectral response of the soil. In recent years, the number of studies on the determination of soil parameters using various methods has been increasing [16-28].

In this study, the compaction parameters of soil brought from an aggregate quarry located in the Karaömerler area of the province of Konya in Türkiye were identified in the laboratory environment. The parameters obtained based on the experimental results were compared to those obtained with image processing methods.

2. Material and Method

The aggregate that was used in the experiments, which was obtained from the Karaömerler aggregate quarry in Konya, was characterized based on methods specified in the Turkish Technical Specification for Highways (KTS). It was seen that the material did not contain residual materials such as vegetal earth, wood, organic matter, waste material, debris, or rubble. To determine the index properties of the soil, sieve analysis, consistency limit analysis, and specific gravity analysis were carried out. The Los Angeles abrasion test was also conducted.

The sieve analysis was conducted in compliance with the ASTM D1140-17 standard, and a granulometric curve was drawn (Figure 1). The physical properties of the soil are given in Table 1.

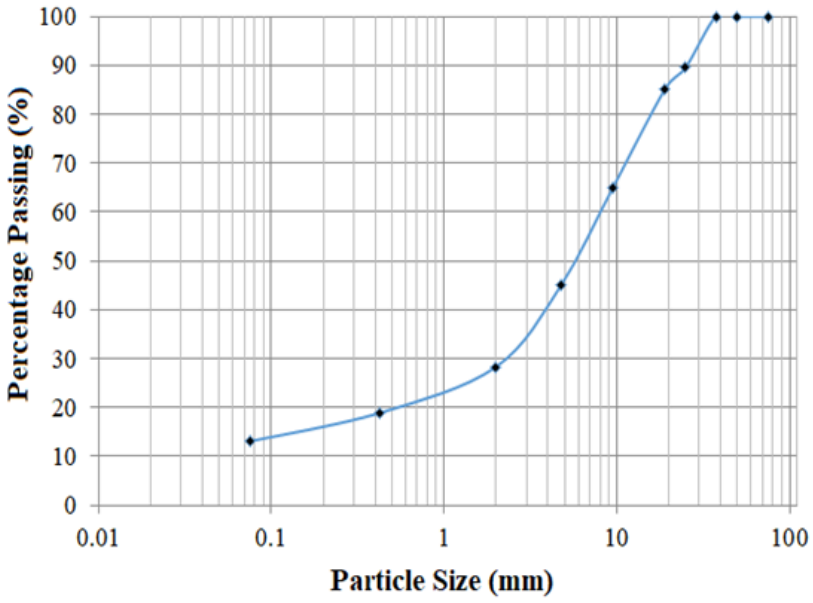

Figure 1. Granulometric curve.

Table 1. Physical properties of the soil.

Specific Gravity	2.65
Liquid Limit, W_L (%)	24.82
Plastic Limit, W_P (%)	21.52
Plasticity Index (IP) (%)	3.30
Soil Class (USCS)	GM
Optimum Water content, ω_{opt} (%)	7.4
Maximum Dry Density, r_{dmax} (g/cm^3)	2.2
Los Angeles Abrasion, (%)	36.16

The experimental results of the sieve analysis and the limit values in the specification are given in Table 2. It was seen that the sieve analysis values satisfied the grading limits in KTS 2013.

Table 2. Sieve analysis test results and specification limits [29].

KTS Grading Limits				
Sieve Aperture		Tip - A	Tip - B	Sieve Analysis
mm	inch	% Passing	% Passing	Results
75	3	100	100	100
50	2	100	100	100
37,5	3/2	85-100	80-100	100
25	1	-	60-90	89.50
19	3/4	70-100	45-80	85.10
9.5	3/8	45-80	30-70	65.00
4.75	No. 4	30-75	25-55	44.97
2	No. 10	-	15-40	28.29
0.425	No. 40	10-25	10-20	18.89
0.075	No. 200	0-12	0-12	13.06

The properties of the material to be used in the granular subbase (GSB) according to KTS 2013 are presented in Table 3. The properties of the soil that was used in the study complied with KTS 2013.

Table 3. Limit values of the GSB material [29].

Experiment	Specification Limit Values	Experimental Standards
Liquid Limit, %	≤ 25	TS 1900-1, AASHTO 89
Plasticity Index, %	≤ 6	TS 1900-1, AASHTO 90
Los Angeles Abrasion, %	≤ 45	TS EN 1097, AASHTO 96

The compaction properties of the soil that was used in the study were also determined using the Standard Proctor experiment. The maximum dry unit weight of the soil (γ_{dmax}) was found 22 kN/m^3, while its optimum water content (w_{opt}) was 7.4% (Figure 2).

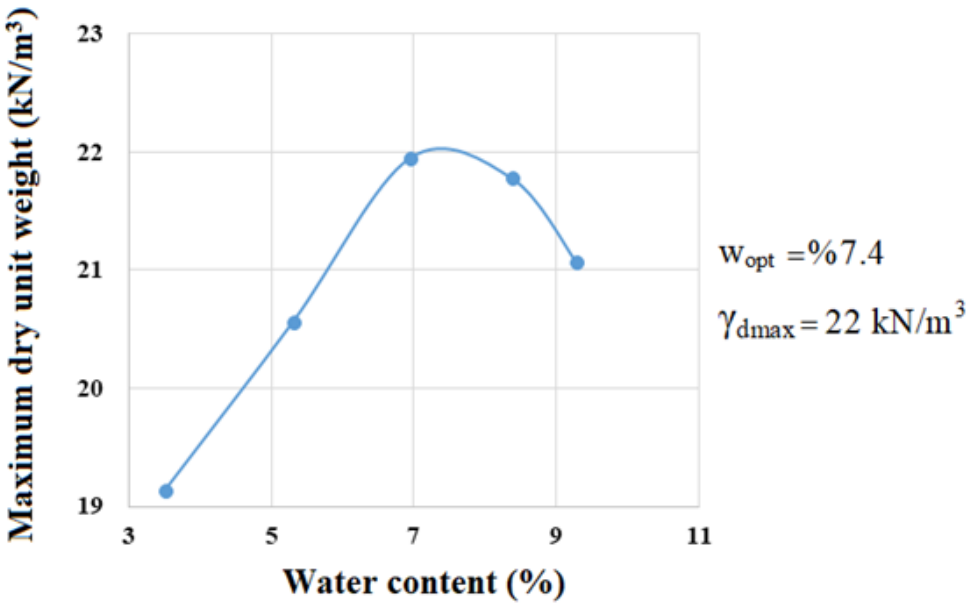

Figure 2. Standard Proctor compaction curve.

To more clearly observe the differences in void ratios in the image analysis, experiments were conducted on the soil specimens with different water contents. For this reason, specimens were prepared at water content values lower than and higher than the optimum water content (4%, 6%, 8%, 10%). The dry unit weight values of the specimens prepared at these values are shown in Table 4.

Table 4. Maximum dry unit weight values at different water contents.

Exp. No.	Water Contents (%)			
	4	6	8	10
	Dry Unit Weight (kN/m³)			
1	19.38	20.92	21.46	20.90
2	19.05	20.10	21.02	20.40
3	19.20	20.30	21.54	20.65
Mean	19.21	20.44	21.34	20.65

Using the maximum dry unit weight values obtained at different water content values, eglobal values were determined (Equation 1). By comparing the eglobal values to the void ratios that were found in the image processing analysis, the reliability of the image processing analysis was determined.

$$e_{global} = \frac{\gamma_s}{\gamma_{d,max}} - 1 \quad (1)$$

Here;

e_{global} : Expected void ratio

g_{dmax} : Maximum unit weight (kN/m³)

g_s : Unit weight of solid (kN/m³)

In the image processing analysis, to determine the void ratios of the soil, compaction specimens were prepared by using an epoxy that had a unit weight close to that of water. To observe the changes in the void ratios, the cross-sections of the compacted soil specimens were photographed, and the horizontal distributions of the void ratios were examined. The specimens that were removed from the molds were kept in the same environment for 24 hours. The specimens that were prepared are shown in Figure 3.

Figure 3. Specimens prepared with epoxy.

As seen in Figure 4, all specimens were cut into 5 pieces with a specimen cutting machine device at the lowest speed. The schema of the horizontal sections is given in Figure 5. The reason for cutting from the regions shown in Figure 5 as Layer 1, Layer 2, and Layer 3 was the aim to identify the compaction in these regions. Calculations and image analysis were not carried out on the top and bottom pieces considering disturbances that occurred after specimen cutting and during compaction.

Figure 4. Cutting of the specimens and the resulting horizontal sections.

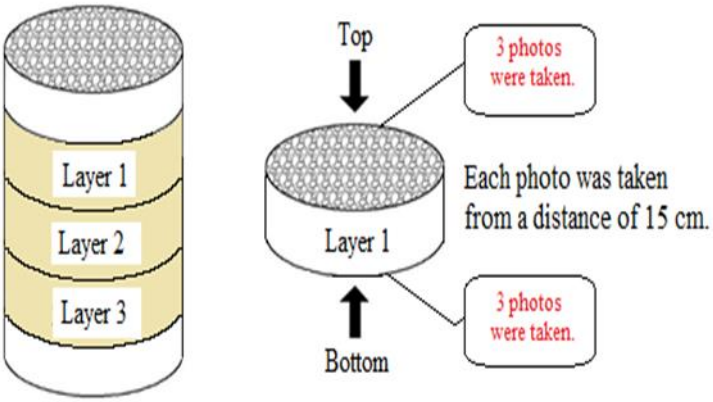

Figure 5. Sample preparation process for image analysis.

The images that were used in this study were taken using a camera with a resolution of 20MP. The obtained images had the dimensions of 3864x5152, a resolution of 350 dpi, and a 24-bit color depth. Eighteen photographs were taken for each void ratio. The simulation results obtained with 18 images for the 8% water content that was found to provide the best outcome are presented in two different sections as visual and statistical results. The flowchart of the method that was used in the study is presented in Figure 6.

Figure 6. Flowchart of the method.

As seen in Figure 6, in the method, first, the original image is downscaled. After this, the image is converted to grayscale. Thresholding is performed on the grayscale image. An epoxy region is selected on the image that is subjected to thresholding using the Region Growing [30] algorithm. The void ratio is calculated using the selected epoxy. The detailed analysis of the method shown in Figure 6 is presented in Figure 7 and Figure 8. While the detailed analysis of the processes carried out until the selection of the epoxy region is given in Figure 7, the details of the void ratio calculation are given in Figure 8.

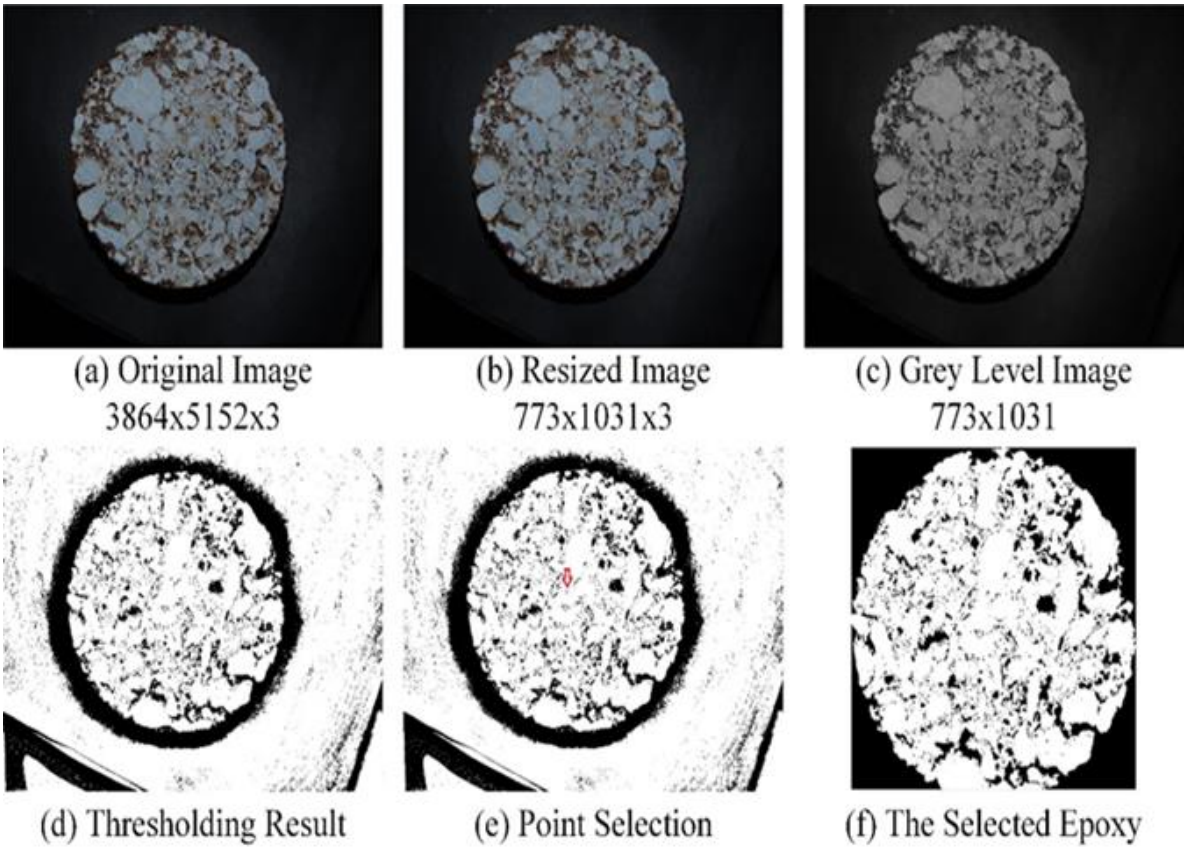

Figure 7. Detailed analysis of epoxy selection.

In the computer vision system that was established, the original image was resized first (Figure 7b). Next, the resized image was converted to grayscale (Figure 7c). The image that was converted to grayscale was subjected to thresholding using the Adaptive Thresholding [31] algorithm (Figure 7d). After thresholding, a point was selected on the epoxy in the image. This point was selected as the starting point of the Region Growing algorithm (Figure 7e). The output image of the Region Growing algorithm, namely the selected epoxy, is seen in Figure 7f. After identifying the epoxy, the void ratio on it was calculated. The details of the void ratio calculations are given in Figure 8.

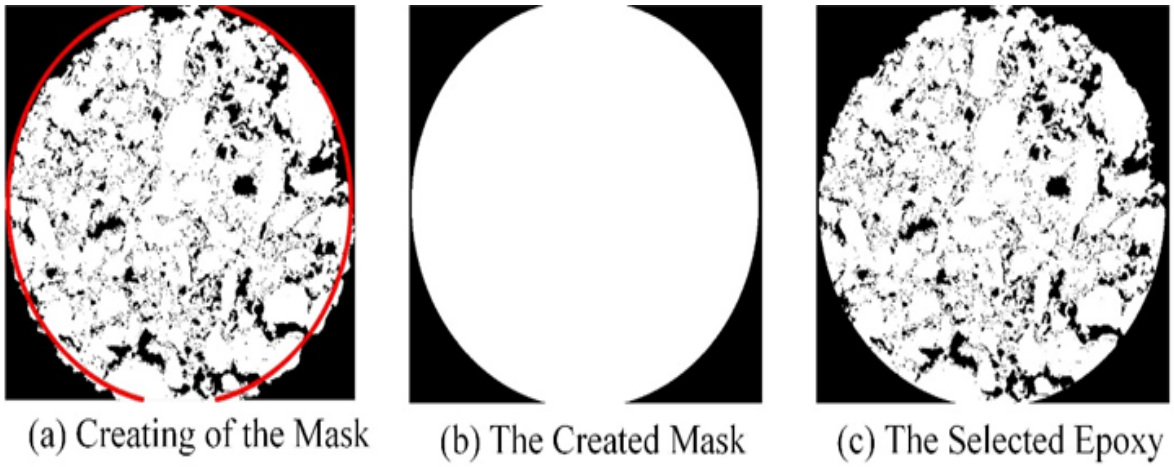

Figure 8. Calculation of void ratios.

After identifying the epoxy, to create a mask with the same dimensions as the epoxy, first, the surroundings of the epoxy and the area of occupies are determined (Figure 8a). Afterward, this area is formed as seen in Figure 8b. On the mask, the white points represent the pixels containing the epoxy, whereas the black points represent the pixels not containing the epoxy. By comparing the two images given in Figure 8b and Figure 8c pixel by pixel, the percentage of the white pixels in the image is found. The void ratio of the epoxy is found by subtracting the obtained value from 100. The visual results that were obtained with the method that was applied are given in Figure 9.

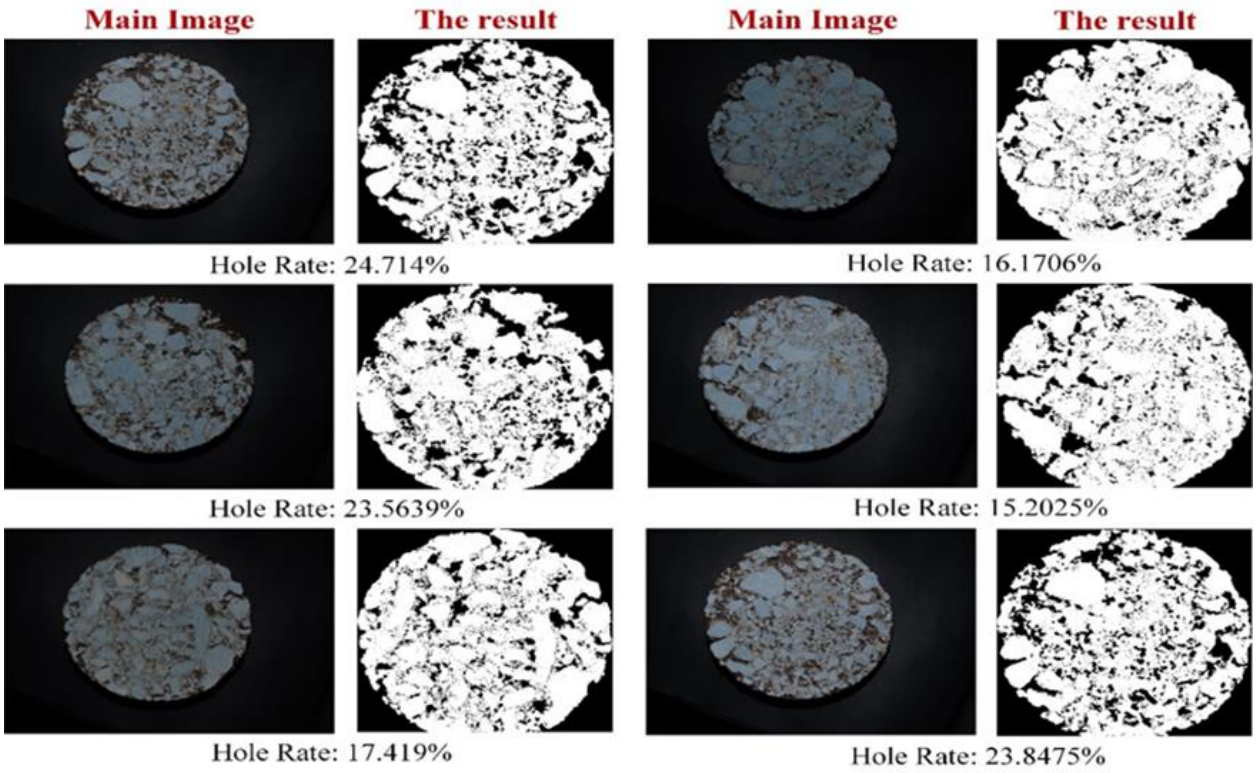

Figure 9. Visual results obtained for different images.

2.1. Experiment Design

The Taguchi method investigates the impacts of parameters on results by conducting a limited number of experiments with the most appropriate orthogonal index chosen by using factors that are effective on the result and can be controlled for an experimental study. Using this method, the cost of the experiment may be kept to a minimum while maximum and lowest values can be approximated from the results of unconducted experiments. In the Taguchi method, specially developed orthogonal index tables are used for designs.

The geotechnical properties of the lightweight fill, which includes EPS (Expanded Polystyrene Foam), waste tires, sand, and cement components, were examined in this study. Using the L_{25} design table with the Taguchi method-specific 5 parameters and 5 levels, experimental studies were carried out. The weight cement/mixture (EPS + waste tire + sand) ratios for the designs shown in Table 5 are 8/1, 10/1, 12/1, 14/1, and 16/1. The amount of waste tire and EPS in the combination ranged from 10% to 50% by weight while the cement/mixture ratio was kept constant.

2.2. Sample Preparation and Experiments

While samples of lightweight fill were being prepared for each design in Table 5, To ensure that the mixes were homogeneous, cement, waste tire, and sand were blended dry in the first stage. The required water was then added to each mixture and well mixed to achieve homogeneity. EPS were added and mixed again (homogeneously) according to the technical specifications of the EPS beads obtained in the laboratory, and the specimens were compacted in three layers in volume-controlled PVC molds of 5 cm diameter and 10 cm height (Figure 10).

Airtight packaging was used for test samples compacted in PVC molds. 7 and 28-day-old spheroids were left at room temperature in a plastic rectangular storage container. 90 unconfined pressure test specimens were prepared for the samples that were extracted from the PVC molds at the end of the curing periods, three for each design, with curing times of 7 and 28 days (Figure 11).

Table 5. Mixtures ratios.

Mixture No	Cement/ Mixture (EPS+ Tire+ Sand)	EPS (%)/(Mixture)	Tire (%)/(Mixture)
1	8/1	10	10
2	8/1	20	20
3	8/1	30	30
4	8/1	40	40
5	8/1	50	50
6	10/1	10	20
7	10/1	20	30
8	10/1	30	40
9	10/1	40	50
10	10/1	50	10
11	12/1	10	30
12	12/1	20	40
13	12/1	30	50
14	12/1	40	10
15	12/1	50	20
16	14/1	10	40
17	14/1	20	50
18	14/1	30	10
19	14/1	40	20
20	14/1	50	30
21	16/1	10	50
22	16/1	20	10
23	16/1	30	20
24	16/1	40	30
25	16/1	50	40

Figure 10. Sample preparation process.

According to ASTM D2166 standard, the unconfined compressive strength test was conducted [28]. The samples (D=50mm; L=100mm) were taken out of their molds and placed into the testing dvice. 0.5 mm/min was selected as the loading speed tests were carried out after the samples had been cured for 7 and 28 days, respectively. The computer was used to keep a record of the load and penetration changes during the experiment.

It was deemed sufficient for the 7-day strength to be more than 0.3 MPa and the 28-day strength to be less than 1.0 MPa since back-cutting is a possibility after the use of lightweight fill materials. CBR and freeze-thaw tests were conducted for the designs (numbered 3-9-10-15-20), whose strengths ranged from 0.3 MPa to 1.0 MPa as a result of the unconfined compressive test. A deep freezer was used to determine the freeze-thaw behavior of the samples. Between -18 and -21 ℃, the freezing procedure was used. The thawing procedure was completed at working room temperature of +21 ℃. There have been 12 freeze-thaw cycles, with 12 hours of waiting between each temperature. After the detached parts of the samples were removed after the freeze-thaw test, unconfined compressive test and CBR tests were performed on the samples before and after freezing-thawing to determine the freeze-thaw behavior. CBR tests were conducted in accordance with TS 1900-2 [29]. Prepared in molds with

a diameter of 150 mm. They were held for cure times of 7 and 28 days. A CBR test equipment with an adjustable piston speed between 0.5 and 5 mm/min was used for the experiments, which were conducted using a digital data acquisition and control unit.

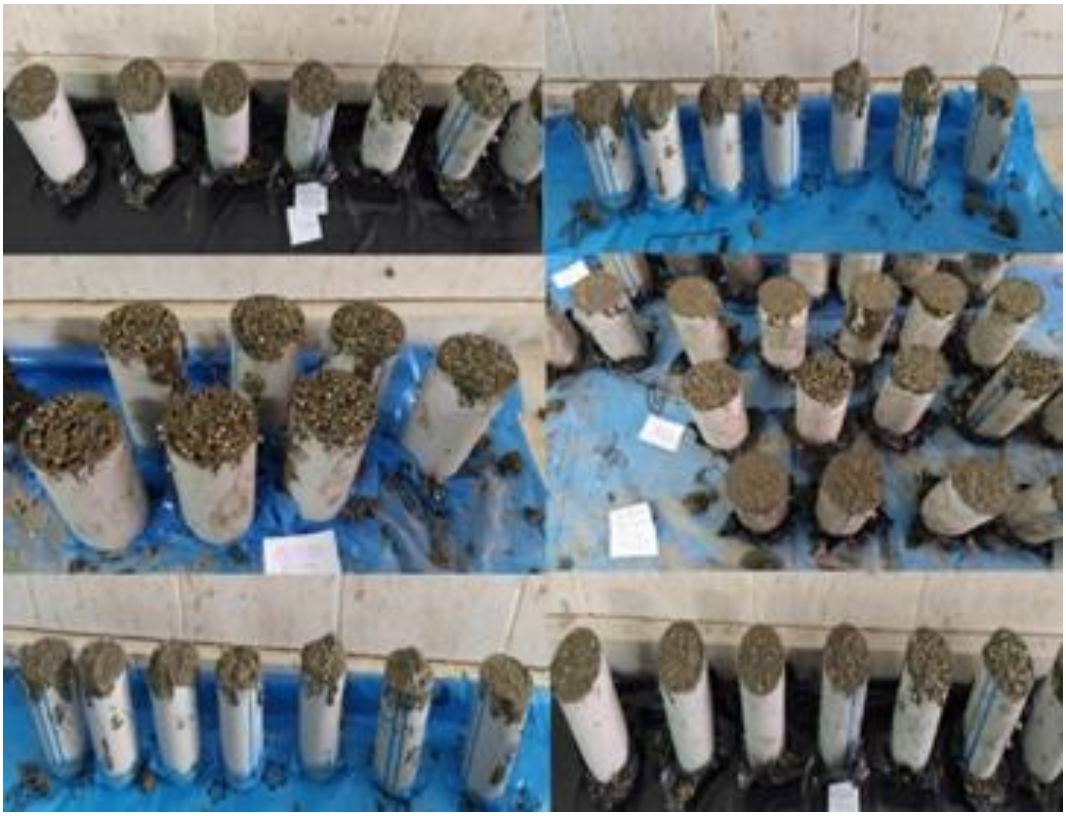

Figure 11. Prepared test samples.

3. Results

The statistical results of the method that is proposed in this study are reported in this section. The proposed method provided the best performance for the 8% water content in Experiment 2. Therefore, the statistical results are presented for Experiment 2 at 8%. The proposed method included two different thresholding methods, manual and adaptive thresholding. In manual thresholding, the images were subjected to thresholding based on a specific value, while the Adaptive Thresholding algorithm was used in the adaptive thresholding process. Table 6 shows the results of the manual thresholding method.

Table 6. Best results for each image.

Image	Simulation Result	Threshold
1st-layer top 1 ph.	23.31	93
1st-layer top 2 ph.	21.03	95
1st-layer top 3 ph.	25.71	70
1st-layer bottom 1 ph.	25.01	70
1st-layer bottom 2 ph.	24.62	63
1st-layer bottom 3 ph.	24.17	75
2nd-layer top 1 ph.	24.38	62
2nd-layer top 2 ph.	24.36	70
2nd-layer top 3 ph.	24.81	70
2nd-layer bottom 1 ph.	23.57	82
2nd-layer bottom 2 ph.	24.95	73
2nd-layer bottom 3 ph.	24.84	62
3rd-layer top 1 ph.	22.11	93
3rd-layer top 2 ph.	24.27	75
3rd-layer top 3 ph.	24.93	85
3rd-layer bottom 1 ph.	22.89	45
3rd-layer bottom 2 ph.	22.93	58
3rd-layer bottom 3 ph.	26.63	65

Table 7 shows the best results for 18 images at different threshold values. A single threshold value was determined by taking the average of the threshold values. Using this threshold value, all images were analyzed again. After the analysis, the void ratio values that were found experimentally and those that were found in simulations were compared, and the accuracy levels of the manual and adaptive thresholding methods in finding the void ratios were obtained.

Table 7. Success rates of the manual and adaptive thresholding methods.

Method	Images	Threshold	Success
Manuel	18 images	72	78.68%
Adaptive	18 images	--	86.12%

As seen in Table 7, the void ratio could be determined at a mean accuracy rate of 78.68% by manual thresholding. In adaptive thresholding, the mean accuracy rate was found 86.12%. Using the adaptive thresholding method, approximately 8% better prediction was achieved. Detailed results are shown in Table 8.

Void ratios were also determined for the specimens containing 4%, 6%, and 10% epoxy by applying the same methods. Based on the proportion of the void ratio values that were obtained as a result of the analysis of 18 photographs taken for each specimen to the e_{global} values, their safety factor values were determined. The results of the image processing analysis that were carried out at different water content values are presented in Table 9. As seen in Table 9, the highest rates in the prediction of the void ratios were achieved in the specimens containing 8% epoxy. High rates were also obtained in the prediction of the void ratios in all other specimens, except for the specimens with a 10% water content. Detailed results are shown in Table 10-13.

Table 8. Image analysis results of the specimens containing 8% epoxy.

Photograph Detail	Void Ratio (e)				Mean Squared Error		
	Expected (e_{global})	Image Analysis Results					
		Exp. 1	Exp. 2	Exp. 3	Exp. 1	Exp. 2	Exp. 3
1st-layer top 1 ph.	24.41	30.8	13.35	12.96	18.78	20.44	20.69
1st-layer top 2 ph.	24.41	27.88	12.16	16.03	13.47	21.17	18.41
1st-layer top 3 ph.	24.41	28.66	11.19	17.41	15.01	21.69	17.11
1st-layer bottom 1 ph.	24.41	21.48	26.9	16.77	11.59	11.3	17.74
1st-layer bottom 2 ph.	24.41	22.28	30.35	17.86	9.97	18.04	16.64
1st-layer bottom 3 ph.	24.41	23.29	24.17	17.18	7.31	3.41	17.34
2nd-layer top 1 ph.	24.41	14.24	33.8	12.95	19.83	23.38	20.69
2nd-layer top 2 ph.	24.41	9.74	27.53	12.25	22.38	12.73	21.11
2nd-layer top 3 ph.	24.41	12.69	33.26	12.01	20.85	22.59	21.25
2nd-layer bottom 1 ph.	24.41	17.83	24.42	20.76	16.67	0.7	12.84
2nd-layer bottom 2 ph.	24.41	20.65	23.98	22.28	13.01	4.56	9.97
2nd-layer bottom 3 ph.	24.41	14.41	23.61	22.75	19.7	6.2	8.85
3rd-layer top 1 ph.	24.41	11.36	14.09	18.97	21.61	19.93	15.36
3rd-layer top 2 ph.	24.41	10.37	24.27	18.99	22.09	2.61	15.34
3rd-layer top 3 ph.	24.41	11.93	18.32	18.79	21.3	16.13	15.58
3rd-layer bottom 1 ph.	24.41	23.05	19.95	18.23	8.03	14.07	16.23
3rd-layer bottom 2 ph.	24.41	23.28	18.19	19.49	7.34	16.28	14.7
3rd-layer bottom 3 ph.	24.41	22.84	19.51	19.73	8.61	14.67	14.37
Mean					15.41	13.88	16.34

Table 9. Image analysis results of the experimental specimens at different epoxy content values.

Water Content (%)	Void Ratio (e)				Safety Factor (GF)		
	Expected (e_{global})	Image Analysis Results (Mean)					
		Exp. 1	Exp. 2	Exp. 3	Exp. 1	Exp. 2	Exp. 3
4	37.95	25.81	25.43	25.81	0.68	0.67	0.68
6	29.65	22.53	16.60	20.16	0.76	0.56	0.68
8	24.41	19.28	22.21	17.58	0.79	0.91	0.72
10	28.33	14.17	15.30	13.88	0.50	0.54	0.49

Table 10. Image analysis results of the specimens containing 4% epoxy.

Photograph Detail	Void Ratio (e)				Mean Squared Error		
	Expected (e_{global})	Image Analysis Results					
		Exp. 1	Exp. 2	Exp. 3	Exp. 1	Exp. 2	Exp. 3
1st-layer top 1 ph.	37.95	22.18	18.14	17.40	0.58	0.48	0.46
1st-layer top 2 ph.	37.95	24.59	32.98	16.60	0.65	0.87	0.44
1st-layer top 3 ph.	37.95	24.12	31.46	12.26	0.64	0.83	0.32
1st-layer bottom 1 ph.	37.95	27.33	24.37	29.54	0.72	0.64	0.78
1st-layer bottom 2 ph.	37.95	23.38	28.99	27.81	0.62	0.76	0.73
1st-layer bottom 3 ph.	37.95	36.22	28.87	26.36	0.95	0.76	0.69
2nd-layer top 1 ph.	37.95	28.89	20.93	26.52	0.76	0.55	0.70
2nd-layer top 2 ph.	37.95	29.72	22.29	28.32	0.78	0.59	0.75
2nd-layer top 3 ph.	37.95	28.10	19.84	30.83	0.74	0.52	0.81
2nd-layer bottom 1 ph.	37.95	30.60	28.74	29.12	0.81	0.76	0.77
2nd-layer bottom 2 ph.	37.95	33.89	29.01	28.23	0.89	0.76	0.74
2nd-layer bottom 3 ph.	37.95	27.12	28.00	32.44	0.71	0.74	0.85
3rd-layer top 1 ph.	37.95	12.35	18.44	22.15	0.33	0.49	0.58
3rd-layer top 2 ph.	37.95	16.90	23.74	20.84	0.45	0.63	0.55
3rd-layer top 3 ph.	37.95	32.59	22.87	28.90	0.86	0.60	0.86
3rd-layer bottom 1 ph.	37.95	21.82	22.97	24.61	0.58	0.61	0.65
3rd-layer bottom 2 ph.	37.95	23.54	32.48	35.06	0.62	0.86	0.92
3rd-layer bottom 3 ph.	37.95	20.92	25.02	26.60	0.55	0.66	0.70
Mean					0.68	0.67	0.68

Table 11. Image analysis results of the specimens containing 6% epoxy.

Photograph Detail	Void Ratio (e)				Mean Squared Error		
	Expected (e_{global})	Image Analysis Results					
		Exp. 1	Exp. 2	Exp. 3	Exp. 1	Exp. 2	Exp. 3
1st-layer top 1 ph.	29.65	24.92	22.97	17.52	0.84	0.77	0.59
1st-layer top 2 ph.	29.65	28.57	21.14	14.93	0.96	0.71	0.50
1st-layer top 3 ph.	29.65	27.49	22.39	19.92	0.93	0.76	0.67
1st-layer bottom 1 ph.	29.65	20.34	23.05	23.23	0.69	0.78	0.78
1st-layer bottom 2 ph.	29.65	22.75	23.41	26.06	0.77	0.79	0.88
1st-layer bottom 3 ph.	29.65	21.92	23.76	25.45	0.74	0.80	0.86
2nd-layer top 1 ph.	29.65	23.71	12.41	25.62	0.80	0.42	0.86
2nd-layer top 2 ph.	29.65	21.59	14.32	28.08	0.73	0.48	0.95
2nd-layer top 3 ph.	29.65	22.75	12.86	28.29	0.77	0.43	0.95
2nd-layer bottom 1 ph.	29.65	15.10	11.39	19.34	0.51	0.38	0.65
2nd-layer bottom 2 ph.	29.65	20.15	11.70	22.30	0.68	0.39	0.75
2nd-layer bottom 3 ph.	29.65	24.69	11.81	17.75	0.83	0.40	0.60
3rd-layer top 1 ph.	29.65	31.91	12.37	19.73	1.08	0.42	0.67
3rd-layer top 2 ph.	29.65	27.79	13.04	20.80	0.94	0.44	0.70
3rd-layer top 3 ph.	29.65	27.16	12.77	21.15	0.92	0.43	0.71
3rd-layer bottom 1 ph.	29.65	10.59	16.40	11.90	0.36	0.55	0.40
3rd-layer bottom 2 ph.	29.65	18.73	15.22	11.03	0.63	0.51	0.37
3rd-layer bottom 3 ph.	29.65	14.81	15.75	11.70	0.50	0.53	0.39
Mean					0.76	0.56	0.68

4. Conclusion

In this study, the compaction parameters of soils brought from the aggregate quarry located in the Karaömerler area of the Sarıcılar Neighborhood in the Selçuklu District of Konya were determined by conducting compaction experiments in the laboratory environment. The parameters obtained as a result of the experiments were compared to the results of the image analysis. For this purpose, photographs were taken to predict the void ratios of the soil that was compacted in Standard Proctor molds. By subjecting the images to a set of processing steps,

their properties in grayscale and in terms of color shades were revealed. These processes were referred to as the Image Analysis Technique throughout the article. The void ratios of the compacted soil specimens were predicted by carrying out regression analysis of the pixel/pixels constituted by the color gray and its shades that were obtained following a set of arithmetic operations on the digital images of the objects (specimens compacted at different water content values). While taking the photographs, the distance between the camera and the objects was kept constant at 15 cm, while the photographs were taken from three different points on each object. Based on these photographs that were obtained from the specimens compacted at different water content values, the void ratios of the specimens were calculated in the computer environment using the MATLAB program.

Table 12. Image analysis results of the specimens containing 8% epoxy.

Photograph Detail	Void Ratio (e)				Mean Squared Error		
	Expected (e_{global})	Image Analysis Results					
		Exp. 1	Exp. 2	Exp. 3	Exp. 1	Exp. 2	Exp. 3
1st-layer top 1 ph.	24.41	30.80	13.35	12.96	1.26	0.55	0.53
1st-layer top 2 ph.	24.41	27.88	12.16	16.03	1.14	0.50	0.66
1st-layer top 3 ph.	24.41	28.66	11.19	17.41	1.17	0.46	0.71
1st-layer bottom 1 ph.	24.41	21.48	26.90	16.77	0.88	1.10	0.69
1st-layer bottom 2 ph.	24.41	22.28	30.35	17.86	0.91	1.24	0.73
1st-layer bottom 3 ph.	24.41	23.29	24.17	17.18	0.95	0.99	0.70
2nd-layer top 1 ph.	24.41	14.24	33.80	12.95	0.58	1.38	0.53
2nd-layer top 2 ph.	24.41	9.74	27.53	12.25	0.40	1.13	0.50
2nd-layer top 3 ph.	24.41	12.69	33.26	12.01	0.52	1.36	0.49
2nd-layer bottom 1 ph.	24.41	17.83	24.42	20.76	0.73	1.00	0.85
2nd-layer bottom 2 ph.	24.41	20.65	23.98	22.28	0.85	0.98	0.91
2nd-layer bottom 3 ph.	24.41	14.41	23.61	22.75	0.59	0.97	0.93
3rd-layer top 1 ph.	24.41	11.36	14.09	18.97	0.46	0.58	0.78
3rd-layer top 2 ph.	24.41	10.37	24.27	18.99	0.42	0.99	0.78
3rd-layer top 3 ph.	24.41	11.93	18.32	18.79	0.49	0.75	0.77
3rd-layer bottom 1 ph.	24.41	23.05	19.95	18.23	0.94	0.82	0.75
3rd-layer bottom 2 ph.	24.41	23.28	18.19	19.49	0.95	0.74	0.80
3rd-layer bottom 3 ph.	24.41	22.84	19.51	19.73	0.93	0.80	0.81
	Mean				0.79	0.91	0.72

Table 13. Image analysis results of the specimens containing 10% epoxy.

Photograph Detail	Void Ratio (e)				Mean Squared Error		
	Expected (e_{global})	Image Analysis Results					
		Exp. 1	Exp. 2	Exp. 3	Exp. 1	Exp. 2	Exp. 3
1st-layer top 1 ph.	28.33	11.11	26.61	5.00	0.39	0.94	0.18
1st-layer top 2 ph.	28.33	10.29	25.73	5.66	0.36	0.91	0.20
1st-layer top 3 ph.	28.33	12.62	25.25	5.21	0.45	0.89	0.18
1st-layer bottom 1 ph.	28.33	24.19	11.26	19.31	0.85	0.40	0.68
1st-layer bottom 2 ph.	28.33	24.56	12.81	19.36	0.87	0.45	0.68
1st-layer bottom 3 ph.	28.33	24.36	12.80	19.39	0.86	0.45	0.68
2nd-layer top 1 ph.	28.33	8.65	13.95	21.89	0.31	0.49	0.77
2nd-layer top 2 ph.	28.33	8.31	11.39	22.09	0.29	0.40	0.78
2nd-layer top 3 ph.	28.33	8.67	11.64	22.12	0.31	0.41	0.78
2nd-layer bottom 1 ph.	28.33	14.63	14.76	11.76	0.52	0.52	0.42
2nd-layer bottom 2 ph.	28.33	14.6	14.38	11.07	0.52	0.51	0.39
2nd-layer bottom 3 ph.	28.33	14.39	14.17	13.98	0.51	0.50	0.49
3rd-layer top 1 ph.	28.33	17.74	13.38	13.07	0.63	0.47	0.46
3rd-layer top 2 ph.	28.33	17.35	13.39	13.32	0.61	0.47	0.47
3rd-layer top 3 ph.	28.33	18.66	13.41	12.95	0.66	0.47	0.46
3rd-layer bottom 1 ph.	28.33	8.74	13.38	10.19	0.31	0.47	0.36
3rd-layer bottom 2 ph.	28.33	9.22	13.28	10.65	0.33	0.47	0.38
3rd-layer bottom 3 ph.	28.33	9.26	13.29	10.40	0.33	0.47	0.37
	Mean				0.50	0.54	0.49

In geotechnical engineering, the relationships of the compaction parameters with the optimum water content and the maximum dry unit weight are important. In preliminary design steps, using these parameters, correlation equations can be calculated in a very short time based on analysis when time is limited, and the resources are insufficient.

In this study, by providing the properties of a granular material that is used in base filling in the foundations of buildings and granular subbases (GSB), reliable results were obtained to a certain extent using image analysis and compaction parameters.

By taking photographs from the horizontal sections of the specimens that were prepared for examination with the Image Analysis Technique (IAT), generally reliable results were obtained with codes prepared using the MATLAB program. The general rate of reliability was approximately 67%.

In the image processing analysis, the highest safety factor values were obtained with the specimens with a water content value of 8%. The prediction accuracy for the void ratios of these specimens was 79.67%.

The reliability rates of the specimens with water content values of 4%, 6%, and 10% were 67.67%, 66.67%, and 51%, respectively. In the experiments that were performed under the same conditions, different safety factor results were observed. The reason for this was that the voids between the grains of the granular material had an irregular structure during compaction.

Funding

This research received no external funding.

Author contributions

Atila Demiröz: Conceptualization, Methodology, **Mücahit Barstugan and Onur Saran:** Data curation, Writing-Original draft preparation, Validation. **Hurşit Battal:** Visualization, Investigation, Writing-Reviewing and Editing.

Conflicts of interest

The authors declare no conflicts of interest.

References

1. Zorluer, I., Icaga, Y., Gucek, S., & Dundar, E. (2020). Consistency analysis of sand cone and nuclear method results in compacted soils. Revista de la construcción, 19(3), 431-442. http://dx.doi.org/10.7764/rdlc.19.3.431
2. Joslin, J. G. (1959). Ohio's typical moisture-density curves. In Symposium on Application of Soil Testing in Highway Design and Construction. ASTM International.
3. Latta Jr, L., & Leonard Jr, J. B. (1978). U.S. Patent No. 4,107,112. Washington, DC: U.S. Patent and Trademark Office.
4. Nagaraj, T. S., & Srinivasa, B. R. (1994). Analysis and prediction of soil behaviour. Taylor & Francis.
5. Blotz, L. R., Benson, C. H., & Boutwell, G. P. (1998). Estimating optimum water content and maximum dry unit weight for compacted clays. Journal of Geotechnical and Geoenvironmental Engineering, 124(9), 907-912. https://doi.org/10.1061/(ASCE)1090-0241(1998)124:9(907)
6. Frost, J. D., & Kuo, C. Y. (1996). Automated determination of the distribution of local void ratio from digital images. Geotechnical Testing Journal, 19(2), 107-117.
7. Sridharan, A., & Nagaraj, H. B. (2005). Plastic limit and compaction characteristics of finegrained soils. Proceedings of the institution of civil engineers-ground improvement, 9(1), 17-22. https://doi.org/10.1680/grim.2005.9.1.17
8. Onal, O., & Ozden, G. (2006). Sayısal görüntü işleme tekniklerinin geoteknikte uygulama örnekleri. Zemin Mekaniği ve Temel Mühendisliği Onbirinci Ulusal Kongresi, 333-340.
9. Soycan, Y. T. (2008). Yapay sinir ağları yaklaşımı ile kompaksiyon parametrelerinin tahmini. Master's Thesis, Niğde Üniversitesi, Niğde, Türkiye
10. Deb, K., Sawant, V., & Kiran, A. (2010). Effects of fines on compaction characteristics of poorly graded sands. International Journal of Geotechnical Engineering, 4(2), 299-304. https://doi.org/10.3328/IJGE.2010.04.02.299-304
11. Sezer, A., Altun, S., & Goktepe, A. B. (2010). Sıkıştırılmış kumların yerel boşluk oranlarının tahmini. İMO Teknik Dergi, 334, 5113-5134

12. Bessa, I. S., Branco, V. T. C., & Soares, J. B. (2012). Evaluation of different digital image processing software for aggregates and hot mix asphalt characterizations. Construction and building materials, 37, 370-378. https://doi.org/10.1016/j.conbuildmat.2012.07.051
13. Çankaya, G., Arslan, M. H., & Ceylan, M. (2013). Görüntü işleme ve yapay sinir ağlari yöntemleri ile betonun basinç dayaniminin belirlenmesi. Selçuk Üniversitesi Mühendislik, Bilim ve Teknoloji Dergisi, 1(1), 1-12.
14. Ören, A. H. (2014). Estimating compaction parameters of clayey soils from sediment volume test. Applied Clay Science, 101, 68-72. https://doi.org/10.1016/j.clay.2014.07.019
15. dos Santos, J. F., Silva, H. R., Pinto, F. A., & Assis, I. R. D. (2016). Use of digital images to estimate soil moisture. Revista Brasileira de Engenharia Agrícola e Ambiental, 20, 1051-1056.
16. Akbulut, S. (2002). Görüntü analizi ile kum tanelerinin fraktal boyutunun belirlenmesi. Pamukkale Üniversitesi Mühendislik Bilimleri Dergisi, 8(3), 329-334.
17. Sinha, S. K., & Wang, M. C. (2008). Artificial neural network prediction models for soil compaction and permeability. Geotechnical and Geological Engineering, 26, 47-64. https://doi.org/10.1007/s10706-007-9146-3
18. Thompson, M. J., & White, D. J. (2008). Estimating compaction of cohesive soils from machine drive power. Journal of Geotechnical and Geoenvironmental Engineering, 134(12), 1771-1777. https://doi.org/10.1061/(ASCE)1090-0241(2008)134:12(1771)
19. Günaydın, O. (2009). Estimation of soil compaction parameters by using statistical analyses and artificial neural networks. Environmental Geology, 57, 203-215. https://doi.org/10.1007/s00254-008-1300-6
20. Sinecen, M., & Makinacı, M. (2010). Agregaların Temel Şekil Özellikleri Kullanılarak Yapay Sinir Ağları Yardımıyla Sınıflandırılması. Pamukkale Üniversitesi Mühendislik Bilimleri Dergisi, 16(2), 149-153
21. Isik, F., & Ozden, G. (2013). Estimating compaction parameters of fine-and coarse-grained soils by means of artificial neural networks. Environmental earth sciences, 69, 2287-2297. https://doi.org/10.1007/s12665-012-2057-5
22. Viji, V. K., Lissy, K. F., Sobha, C., & Benny, M. A. (2013). Predictions on compaction characteristics of fly ashes using regression analysis and artificial neural network analysis. International Journal of Geotechnical Engineering, 7(3), 282-291. https://doi.org/10.1179/1938636213Z.00000000036
23. Singh, B., Sihag, P., & Singh, K. (2017). Modelling of impact of water quality on infiltration rate of soil by random forest regression. Modeling Earth Systems and Environment, 3, 999-1004. https://doi.org/10.1007/s40808-017-0347-3
24. Ardakani, A., & Kordnaeij, A. (2019). Soil compaction parameters prediction using GMDH-type neural network and genetic algorithm. European Journal of Environmental and Civil Engineering, 23(4), 449-462. https://doi.org/10.1080/19648189.2017.1304269
25. Akyildiz, H., & Akbaş, E. (2020). Basit ve çoklu regresyon analizleri ile kompaksiyon parametrelerinin tahmin edilmesi ve F testi ile anlamlılığının incelenmesi. Engineering Sciences, 15(4), 186-195.
26. Toksöz, D., & Yilmaz, I. (2019). İnce taneli zeminler için önerilen bulanık sınıflama sürecinin bir uygulaması. Pamukkale Üniversitesi Mühendislik Bilimleri Dergisi, 26(3), 535-544.
27. Karslioğlu, A., Mert, A. A., & Onur, M. İ. (2021). Zemin özelliklerinin belirlenmesinde yeni trendler. Avrupa Bilim ve Teknoloji Dergisi, (28), 998-1007. https://doi.org/10.31590/ejosat.1012397
28. Nuray, S. E., Gençdal, H. B., & Arama, Z. A. (2021). Zeminlerin kıvam ve kompaksiyon özelliklerinin tahmininde rastgele orman regresyonu yönteminin uygulanabilirliği. Mühendislik Bilimleri ve Tasarım Dergisi, 9(1), 265-281. https://doi.org/10.21923/jesd.804446
29. Karayolları Genel Müdürlüğü. (2023). Karayolları Teknik Şartnamesi. Ankara, Türkiye.
30. Hojjatoleslami, S. A., & Kittler, J. (1998). Region growing: a new approach. IEEE Transactions on Image processing, 7(7), 1079-1084. https://doi.org/10.1109/83.701170
31. Bradley, D., & Roth, G. (2007). Adaptive thresholding using the integral image. Journal of Graphics Tools, 12(2), 13-21. https://doi.org/10.1080/2151237X.2007.10129236